

1 Morphologic and Morphometric Differences between Gullies Formed 2 in Different Substrates on Mars: New Insights into the Gully 3 Formation Processes

4 Rishitosh K. Sinha^{1,2}, Dwijesh Ray¹, Tjalling De Haas³, Susan J. Conway⁴, Axel Noblet⁴

5 ¹ Physical Research Laboratory, Ahmedabad 380009, Gujarat, India

6 ² Indian Institute of Technology, Gandhinagar 382355, Gujarat, India

7 ³ Faculty of Geoscience, Universiteit Utrecht, Princetonlaan 8a, 3584 CB Utrecht, the Netherlands

8 ⁴ Nantes Université, Université d'Angers, Le Mans Université, CNRS UMR 6112 Laboratoire de Planétologie et Géosciences,
9 France

10

11 *Correspondence to:* Rishitosh K. Sinha (rishitosh@prl.res.in)

12 **Abstract.** Martian gullies are kilometer-scale geologically young features with a source alcove, transportation channel, and
13 depositional fan. On the walls of impact craters, these gullies typically incise into bedrock or surfaces modified by latitude
14 dependent mantle (LDM; inferred as consisting ice and admixed dust) and glaciation. To better understand the differences in
15 alcoves and fans of gullies formed in different substrates and infer the flow types that led to their formation, we have analyzed
16 the morphology and morphometry of 167 gully systems in 29 craters distributed between 30°S and 75°S. Specifically we
17 measured length, width, gradient, area, relief, and relief ratio of alcove and fan, Melton ratio, relative concavity index, and
18 perimeter, form factor, elongation ratio and circularity ratio of the alcoves. Our study reveals that alcoves formed in
19 LDM/glacial deposits are more elongated than the alcoves formed in bedrock, and possess a distinctive V-shaped cross section.
20 We have found that mean gradient of fans formed by gullies sourced in bedrock is steeper than the mean gradient of fans of
21 gullies sourced in LDM/glacial deposits. These differences between gullies were found to be statistically significant and
22 discriminant analysis has confirmed that alcove perimeter, alcove relief and fan gradient are the most important variables for
23 differentiating gullies according to their source substrates. The comparison between the Melton ratio, alcove length and fan
24 gradient of Martian and terrestrial gullies reveals that Martian gully systems were likely formed by terrestrial debris-flow like
25 processes. It is likely that the present-day sublimation of CO₂ ice on Mars provided the adequate flow fluidization for the
26 formation of deposits akin to terrestrial debris-flow like deposits.

Deleted: melton

Deleted: melton

27 1 Introduction

28 Gullies are found on steep slopes polewards of about 30° latitude in both hemispheres on Mars and manifest as kilometer-
29 scale, geologically young features (formed within the last few million years) comprising an alcove, channel, and depositional
30 fan (Malin and Edgett, 2000; Dickson et al., 2007; Reiss et al., 2004; Schon et al., 2009). Gullies occur in a wide assortment

33 of settings, varying from the walls and central peaks of craters to walls of valleys, and steep faces of dunes, hills and polar pits
34 (e.g. Balme et al., 2006; Dickson et al., 2007; Dickson and Head, 2009; Conway et al., 2011, 2015; Harrison et al., 2015). On
35 the walls of craters, gullies are found to have incised into the (1) surfaces covered by latitude dependent mantle (LDM; e.g.
36 Mustard et al., 2001; Dickson et al., 2012, 2015), (2) surfaces modified by former episodes of glaciation (Hubbard et al., 2011;
37 Souness et al., 2012; Souness and Hubbard, 2012; Sinha and Vijayan, 2017), and (3) bedrock (e.g. Johnsson et al., 2014; de
38 Haas et al., 2019a; Sinha et al., 2020). Detailed investigation of the gullies formed over these different substrates is key to
39 understanding the intricacies of past processes by which these gullies have formed on Mars (Conway et al., 2015; de Haas et
40 al., 2019a).

41 A variety of models have been proposed to explain the formation of gullies, which include: (1) dry flows triggered by
42 sublimation of CO₂ frost (e.g. Cedillo-Flores et al., 2011; Dundas et al., 2012, 2015; Pilorget and Forget, 2016; de Haas et al.,
43 2019b), (2) debris-flows of an aqueous nature (e.g. Costard et al., 2002; Levy et al., 2010; Conway et al., 2011; Johnsson et
44 al., 2014; de Haas et al., 2019a; Sinha et al., 2020), and (3) fluvial flows (e.g. Heldmann and Mellon, 2004; Heldmann et al.,
45 2005; Dickson et al., 2007; Reiss et al., 2011). To better understand the gully formation processes, morphometric investigation
46 of gullies formed over different substrates needs to be undertaken at a level of detail previously not attempted.

47 The global distribution of gullies shows a spatial correlation with the landforms indicative of glaciation and LDM deposition
48 on Mars (e.g. Levy et al., 2011; Dickson et al., 2015; Harrison et al., 2015; Conway et al., 2018; de Haas et al., 2019a; Sinha
49 et al., 2020). With respect to glacial landforms, many gullies have formed into viscous flow features (VFF) and they are found
50 in the same extent of latitudes (e.g. Arfstrom and Hartmann, 2005; de Haas et al., 2018). VFFs are defined as an umbrella term
51 for glacial-type formations covering a broad range of landforms that include lobate debris aprons, concentric crater fill, and
52 lineated valley fills (e.g. Squyres, 1978; Levy et al., 2009; Baker et al., 2010; Hargitai, 2014). Together, they are inferred to
53 be similar to terrestrial debris-covered glaciers (Conway et al., 2018). With respect to LDM, gullies are mostly found on the
54 pole-facing slopes of crater walls at lower mid-latitudes (30-45°) (e.g. Balme et al. 2006; Kneissl et al. 2010; Harrison et al.
55 2015; Conway et al. 2017), wherein, LDM is found to be dissected (e.g. Mustard et al., 2001; Milliken et al., 2003; Head et
56 al., 2003). In the higher latitudes (>45°), LDM is found to be continuous (e.g. Kreslavsky and Head, 2000), and gullies are
57 evident at both the pole and equator facing slopes (e.g. Balme et al. 2006; Kneissl et al. 2010; Harrison et al. 2015; Conway et
58 al. 2017). Gullies formed on the formerly glaciated walls of craters are fed from alcoves that do not extend up to the crater rim,
59 and appear elongated to V-shaped, implying gully-channel incision into ice-rich, unlithified sediments (e.g. Aston et al., 2011;
60 de Haas et al., 2019a). The alcoves, channels and fan deposits of gullies formed within craters covered by a smooth drape of
61 LDM, are usually found to have experienced multiple episodes of LDM covering and subsequent reactivation of some of the
62 pre-existing channels or formation of fresh channels within the draped LDM deposits (e.g. Dickson et al., 2015; de Haas et al.,
63 2019a). Additionally, there are gullies that directly emanate from well-defined bedrock alcoves that cut into the crater rim in
64 the absence of LDM and/or glacial deposits (e.g. Johnsson et al., 2014; de Haas et al., 2019a; Sinha et al., 2020). Gullies

Deleted: cover

66 formed in these craters have alcoves with sharply defined crests and spurs, exposing the underlying bedrock, and meter-sized
67 boulders are found throughout the gully system (e.g. Johnsson et al., 2014; de Haas et al., 2019a; Sinha et al., 2020). Further,
68 De Haas et al., 2015a found that the stratigraphy of the fans whose source area was in bedrock were more boulder-rich than
69 those fans fed by catchments in LDM. The findings in these studies suggest that a more detailed investigation of the
70 morphology and morphometry of the gullies formed over contrasting substrates is important for improving our understanding
71 of the formative mechanisms of gullies.

72 In this work, we focus on addressing the following research questions:

73 (1) Do the morphology and morphometry of gully systems formed in different substrates differ (i.e. LDM/glacial deposits and
74 bedrock)?

75 (2) How do the morphometric characteristics of gullies formed on Mars compare to those formed by a range of processes on
76 Earth, and what does that tell us about the formative processes of Martian gullies?

77 To parameterize the morphometry we will primarily study long profiles. Previously, only a few studies have analyzed the
78 morphometric characteristics of the gullies by studying long profiles of gullies (e.g. Yue et al., 2014; Conway et al., 2015; De
79 Haas et al., 2015a; Hobbs et al., 2015). These studies have focused observations on a part of the gully system and suggested
80 that the differences in the properties of substrate into which the gullies incise play a significant role in promoting the flows
81 that led to gully formation. Hence, for a more detailed differentiation of the gully types and interpretation of the dominant flow
82 type that led to gully formation on Mars, quantification of the morphometric characteristics of the entire gully system is crucial.

83 **2 Study sites and datasets**

84 We characterize the morphology and morphometry of gullies in 29 craters distributed over the southern hemisphere between
85 30° S and 75° S latitude (Fig. 1). These 29 craters are selected based on the availability of publicly released High Resolution
86 Imaging Science Experiment (HiRISE) stereo-pair based digital terrain model (DTM) or the presence of suitable HiRISE
87 stereo-pair images to produce a DTM ourselves. The HiRISE stereo-pair images are usually ~0.25 - 0.5 m/pixel (McEwen et
88 al., 2007), so the DTM post spacing is ~1-2 m with vertical precision in the range of tens of centimeters (Kirk et al., 2008).
89 Among the 29 gullied craters, publicly released DTMs are available for 25 craters
90 (<https://www.uahirise.org/hiwish/maps/dtms.jsp> - last accessed 18th September 2021) (Table 1). For the remaining 4 craters,
91 DTMs are produced with the software packages USGS ISIS and BAE Systems SocetSet (Table 1) (Kirk et al., 2008). We
92 investigated HiRISE images of these 29 gullied craters for detailed morphological characterization of the substrate into which
93 the crater wall gullies incise (Table 1).

94

95

96 **Table 1.** Summary of the craters included in this study, their locations, number of gullies investigated from the crater, substrate
 97 on the crater wall in which gullies have incised, key morphological attributes of the substrate, and IDs of HiRISE imagery and
 98 DTM used for morphological and morphometric investigation of gullies in these craters.

Deleted: diameter

Crater	Latitude	Longitude	No. of gullies	Substrate	Key morphological attributes	HiRISE ID	HiRISE DTM ID
Artik	34.8° S	131.02° E	<u>2</u>	LDM/glacial deposits	Polygons, V-shaped incisions, arcuate ridges, small-scale lobate debris aprons (LDAs) on the floor	ESP_020740_1450	DTEEC_012459_1450_012314_1450_A01
Asimov	47.53° S	4.41° E	<u>4</u>	LDM/glacial deposits	Polygons, V-shaped incisions, mantled alcoves/channels/fans, arcuate ridges, small-scale LDAs inside valleys	ESP_012912_1320	DTEEC_012912_1320_012767_1320_A01
Bunnik	38.07° S	142.07° W	<u>8</u>	LDM/glacial deposits	Polygons, V-shaped incisions, mantled alcoves/channels/fans, arcuate ridges	ESP_047044_1420	DTEEC_002659_1420_002514_1420_U01
Corozal	38.78° S	159.48° E	<u>6</u>	LDM/glacial deposits	Polygons, mantled alcoves/channels/fans, arcuate ridges, small-scale LDAs on the floor	PSP_006261_1410	DTEEC_006261_1410_014093_1410_A01
Dechu	42.23° S	158° W	<u>8</u>	LDM/glacial deposits	Polygons, mantled alcoves/channels/fans, arcuate ridges, small-scale LDAs on the floor	PSP_006866_1375	DTEED_023546_1375_023612_1375_A01
Dunkassa	37.46° S	137.06° W	<u>5</u>	LDM/glacial deposits	Polygons, V-shaped incisions, mantled alcoves/channels/fans, arcuate ridges, small-scale LDAs on the floor	ESP_032011_1425	DTEEC_039488_1420_039343_1420_A01
Hale	35.7° S	36.4° W	<u>8</u>	LDM/glacial deposits	Polygons, V-shaped incisions, mantled alcoves/channels/fans, talus slope deposits	PSP_003209_1445	DTEEC_002932_1445_003209_1445_A01
Langtang	38.13° S	135.95° W	<u>5</u>	LDM/glacial deposits	Polygons, V-shaped incisions, mantled alcoves/channels/fans, arcuate ridges, small-scale LDAs on the floor	ESP_030099_1415	DTEEC_024099_1415_023809_1415_U01

Formatted Table

Moni	46.97° S	18.79° E	<u>5</u>	LDM/glacial deposits	Partly infilled alcoves, mantled fan surfaces, arcuate ridges	ESP_056862_1325	DTEEC_007110_1325_006820_1325_A01
Nybyen	37.03° S	16.66° W	<u>8</u>	LDM/glacial deposits	Polygons, mantled alcoves/channels/fans, arcuate ridges	ESP_059448_1425	DTEEC_006663_1425_011436_1425_A01
Palikir	41.56° S	157.87° W	<u>5</u>	LDM/glacial deposits	Polygons, V-shaped incisions, mantled alcoves/channels/fans, arcuate ridges, small-scale LDAs on the floor	ESP_057462_1380	DTEEC_005943_1380_011428_1380_A01
Penticton	38.38° S	96.8° E	<u>7</u>	LDM/glacial deposits	Polygons, V-shaped incisions, mantled alcoves/channels/fans, arcuate ridges, small-scale LDAs on the floor	ESP_029062_1415	DTEEC_001714_1415_001846_1415_U01
Selevac	37.37° S	131.07° W	<u>8</u>	LDM/glacial deposits	Polygons, mantled alcoves/channels/fans, small-scale flows on the floor	ESP_045158_1425	DTEEC_003252_1425_003674_1425_A01
Raga	48.1° S	117.57° W	<u>4</u>	LDM	Polygons, mantled alcoves/channels/fans	ESP_041017_1315	DTEEC_014011_1315_014288_1315_A01
Roseau	41.7° S	150.6° E	<u>1</u>	LDM	Polygons, mantled alcoves/channels/fans	ESP_024115_1380 / ESP_011509_1380	ESP_024115_1380_ESP_011509_1380*
Taltal	39.5° S	125.8° W	<u>7</u>	LDM/glacial deposits	Polygons, V-shaped incisions, mantled alcoves/channels/fans, arcuate ridges, small-scale LDAs on the floor	ESP_037074_1400 / ESP_031259_1400	ESP_037074_1400_ESP_031259_1400*
Talu	40.34° S	20.11° E	<u>7</u>	LDM/glacial deposits	Polygons, V-shaped incisions, mantled alcoves/channels/fans, arcuate ridges, small-scale LDAs on the floor	ESP_011817_1395	DTEEC_011817_1395_011672_1395_O01
Triolet	37.08° S	168.02° W	<u>4</u>	LDM/glacial deposits	Polygons, V-shaped incisions, mantled alcoves/channels/fans, arcuate ridges, small-scale LDAs on the floor	ESP_047190_1425	DTEEC_023586_1425_024008_1425_A01
Unnamed crater	32.31° S	118.55° E	<u>4</u>	LDM/glacial deposits	Polygons, mantled alcoves/channels/fans	PSP_006869_1475	DTEEC_021914_1475_022336_1475_U01

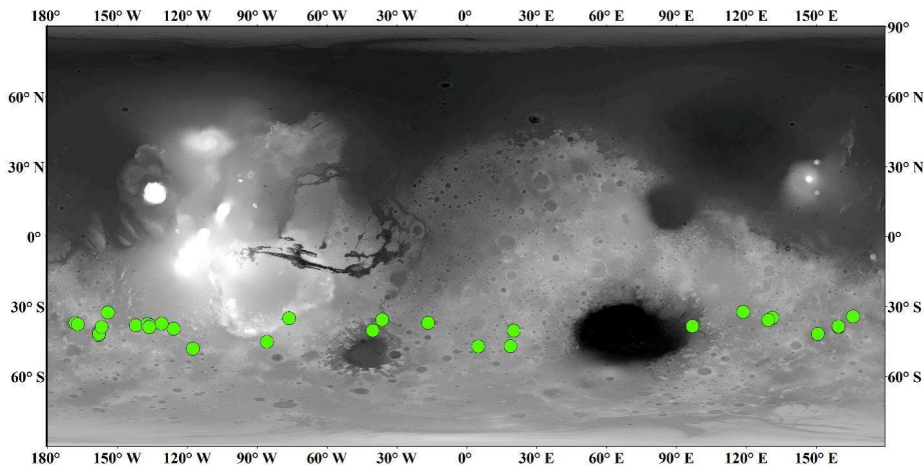
					s, arcuate ridges, small-scale LDAs on the floor		
Unnamed crater in the Argyre basin	40.3° S	40.4° W	<u>6</u>	LDM/glacial deposits	Polygons, mantled alcoves/channels/fans, arcuate ridges, small-scale LDAs on the floor	ESP_032047_1395	DTEEC_012795_1395_013507_1395_A01
Unnamed crater in the Newton basin	38.8° S	156.8° W	<u>5</u>	LDM	Polygons, V-shaped incisions, mantled alcoves/channels/fans	PSP_002686_1410	DTEEC_002620_1410_002686_1410_A01
Unnamed crater north of Corozal crater	38.53° S	159.44° E	<u>5</u>	LDM/glacial deposits	Polygons, mantled alcoves/channels/fans, small-scale LDAs on the floor	ESP_020884_1410	DTEEC_020884_1410_020950_1410_A01
Unnamed crater-1 in the Terra Sirenum	32.55° S	154.11° W	<u>2</u>	LDM	Mantled alcoves/channels/fans	PSP_007380_1470	DTEEC_010597_1470_007380_1470_U01
Unnamed crater-2 in the Terra Sirenum	38.88° S	136.36° W	<u>6</u>	LDM/glacial deposits	Polygons, V-shaped incisions, mantled alcoves/channels/fans, arcuate ridges, small-scale LDAs on the floor	ESP_020407_1410	DTEEC_022108_1410_022385_1410_A01
Istok	45.1° S	85.82° W	<u>8</u>	Bedrock	Alcove cut directly into the original crater-wall material, clasts embedded into fresh deposits on fan	ESP_056668_1345	DTEEC_040607_1345_040251_1345_A01
Galap	37.66° S	167.07° W	<u>8</u>	Bedrock	Alcove cut directly into the original crater-wall material, clasts embedded into fresh deposits on fan	ESP_059770_1420	DTEEC_048983_1420_048693_1420_U01
Gasa	35.73° S	129.4° E	<u>7</u>	Bedrock	Alcove cut directly into the original crater-wall material, clasts embedded into fresh deposits on fan	ESP_057491_1440	DTEEC_021584_1440_022217_1440_A01
Los	35.08° S	76.23° W	<u>7</u>	Bedrock	Alcove cut directly into the original crater-wall material,	ESP_020774_1445 / ESP_050127_1445	ESP_020774_1445_ESP_050127_1445*

					clasts embedded into fresh deposits on fan		
Unnamed crater-3 in the Terra Sirenum	34.27° S	165.71° E	<u>7</u>	Bedrock	Alcove cut directly into the original crater-wall material, clasts embedded into fresh deposits on fan	ESP_049261_1455 / ESP_049828_1455	ESP_049261_1455_ ESP_049828_1455*

100

101 (*) DTMs are produced with the software packages USGS ISIS and BAE Systems SocetSet.

102



103 Figure 1: Locations of craters analyzed in this study (green circles). Background: Mars Orbiter Laser Altimeter gridded data, where
 104 white is high elevation and black is low elevation, credit MOLA Science Team/NASA/JPL.

105

106 **3 Approach**

107 **3.1 Identification of substrate**

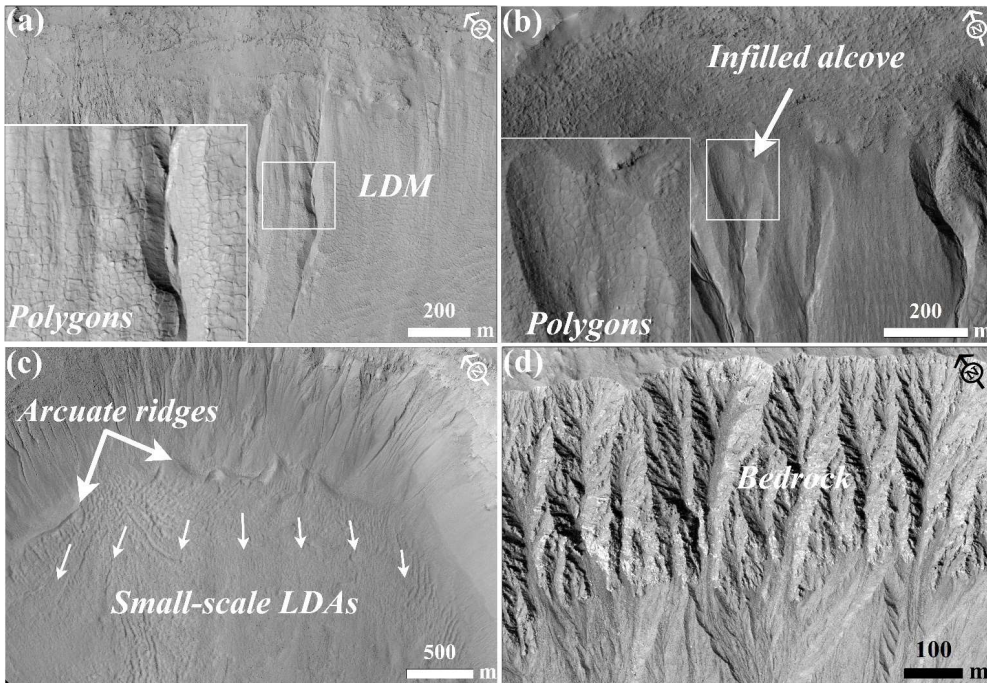
108 The substrate into which the gullies have incised is identified based on the following criteria:

- 109 1. LDM/glacial deposits: Any crater whose gullies incise walls that appear to be softened by the drape of smooth mantling
 110 material with polygonal cracks is inferred to have LDM as the substrate within which gullies have incised (e.g. Mustard et al.,

111 2001; Kreslavsky and Head, 2002; Levy et al., 2009a; Conway et al., 2018; de Haas et al., 2019a) (Fig. 2a). The alcoves on
 112 the walls of these craters may be partially to completely filled by LDM, and in some cases, polygonized LDM materials may
 113 be seen covering the alcove walls (e.g. Christensen, 2003; Conway et al., 2018; de Haas et al., 2019a). These infilled alcoves
 114 on the crater walls are not the alcoves of gullies formed within the LDM substrate; instead, they represent the alcoves that were
 115 formed prior to the LDM emplacement epoch. Additionally, gullied craters that show evidence in the form of arcuate ridges at
 116 the foot of the walls and VFFs that cover part or the entire crater floor are inferred to have been modified by one or multiple
 117 episodes of glaciation (e.g. Arfstrom and Hartmann, 2005; Head et al., 2010; Milliken et al., 2003; Hubbard et al., 2011). These
 118 craters host gullies that are often partially or fully covered by LDM deposits.

119 2. Bedrock: Craters where the features listed in LDM/glacial deposits are absent and where rocky material is visible extending
 120 downwards from the crater rim. This rocky material usually outcrops as spurs and can be layered or massive. The slopes can
 121 be smooth or covered with boulders, with concentrations of boulders at the slope toe.

Deleted: 1



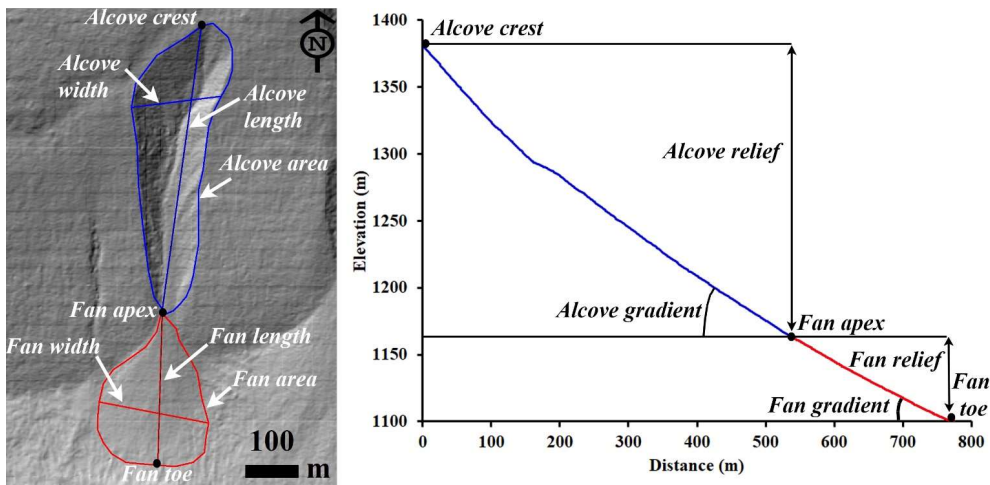
122

124 **Figure 2:** Examples of morphological evidence used to identify LDM, glacial deposits, and bedrock. (a) Smooth mantling material
 125 inferred as LDM draped on the wall of Talu crater on the basis of polygonal cracks formed in the material. The bigger box is an
 126 expanded view of the polygons seen over the region outlined by the smaller box. (HiRISE image ESP_011817_1395). (b) An infilled
 127 alcove on the wall of an unnamed crater-2 in the Terra Sirenum. Evidence of polygons in the infilled material suggests presence of
 128 LDM deposits draped on the wall. The region shown in smaller box is expanded in the bigger box to show evidence of the polygons.
 129 (HiRISE image ESP_020407_1410). (c) Glaciation inferred in the Corozal crater on the basis of arcuate ridges formed at the foot of
 130 the crater wall and small-scale LDAs on the crater floor. Arrows indicate the downslope flow of LDAs on the floor. (HiRISE image
 131 PSP_006261_1410). (d) Exposed fractured bedrock identified on the walls of Istok crater within which alcoves have incised. (HiRISE
 132 image ESP_056668_1345). HiRISE image credit: NASA/JPL /University of Arizona.

133

134 3.2 Morphometric variables

135 The measurements we made of each gully system include alcove area, alcove perimeter, alcove length, alcove width, alcove
 136 gradient, fan area, fan length, fan width, and fan gradient (Fig. 3). In total, we derived 18 morphometric variables to
 137 characterize each gully fan and its alcove. The morphometric variables are classified into geometry, relief, gradient, and
 138 dimensionless variables and they are calculated with established mathematical equations shown in Table 2. For the gradient
 139 measurement using the DTM, the topographic profile from (1) crest of the alcove to the apex of the fan was extracted for the
 140 alcove, and (2) apex to foot of the fan was extracted for the fan.



141

142 **Figure 3:** Examples of morphometric variables estimated in this work. Left panel: HiRISE DTM (Id:
 143 DTEEC_002659_1420_002514_1420) based hillshade. HiRISE DTM credit: NASA/JPL /University of Arizona. Right panel:

144 **Topographic profile: blue profile represents the topography of gully alcove from alcove top to fan apex and red profile represents**
 145 **the profile of gully fan from fan apex to fan toe.**

146

147

148 **Table 2.** Set of morphometric variables extracted from the studied gully systems and their formulas and/or description of
 149 method.

Morphometric variable	Formula and/or description of method	References
Alcove length and width	Measured in km	Tomczyk, 2021
Alcove area	Measured in km ²	Tomczyk, 2021
Fan length and width	Measured in km	Tomczyk, 2021
Fan area	Measured in km ²	Tomczyk, 2021
Melton ratio	(Alcove relief)/(Alcove area ^{0.5})	Melton, 1957
Relative concavity index (RCI)	Concavity Index/(maximum relief between the uppermost and lowermost points along the gully fan profile/2). Concavity Index is estimated as $\sum (H_i^* - H_i) / N$, where H_i^* is the elevation along the straight line, H_i is the elevation along the gully fan profile, N is the total number of measurement points.	Langbein, 1964; Phillips and Lutz, 2008
Alcove gradient	Measured in (°)	Tomczyk, 2021
Fan gradient	Measured in (°)	Tomczyk, 2021
Alcove relief	Measured in km	Tomczyk, 2021
Fan relief	Measured in km	Tomczyk, 2021
Relief ratio (alcove and fan)	Alcove/fan relief divided by the length of the alcove/fan	Schumm, 1956a, b
Perimeter	Measured in km	Schumm, 1956a, b
Form factor	Alcove area divided by the square of the length of the alcove	Horton, 1932
Elongation ratio	Diameter of a circle of the same area as the alcove divided by the maximum alcove length	Schumm, 1956a, b
Circularity ratio	Alcove area divided by the area of the circle having the same perimeter as the alcove perimeter	Miller, 1953

Formatted Table

150

151 3.3 Gully system selection for morphometric measurements

152 We have selected only those gully systems for morphometric measurements in which: (i) the depositional fan from an alcove-
 153 channel system is not superimposed by or interfingering with the fans from the neighboring channels, (ii) there is clear
 154 association between the primary channel emanating from the alcove that extends downslope and then deposit its respective
 155 fan, (iii) no evidence of extensive cross-cutting is seen with the neighboring channels on the walls, (iv) no evidence of extensive
 156 mantling by dust/aeolian deposits is apparent, and (v) no evidence of channel/fan superposition on any topographic obstacle
 157 on the walls or the floor of the crater is apparent, which may have influenced the morphometry. If in any case the fans

Deleted: eventually influence the morphometric measurements

159 ~~superimpose or channels cross-cut, we have carefully demarcated the alcove-channel-fan boundary, to minimize the~~
160 ~~inaccuracies in the measurements.~~ Note that the selection of the gully ~~systems~~ was also constrained by the coverage of HiRISE
161 DTM that was used for morphometric analysis.

Deleted: fans

162 3.4 Statistical analysis of morphometric variables

163 We have two groups of gullies in our study: (1) gullies whose source area is incised into LDM/glacial deposits and (2) gullies
164 whose source area is incised into the bedrock. ~~First, for both the groups we have calculated descriptive statistics for each of~~
165 the morphometric variables shown in Table 2. The significance of the difference between the values of each of the
166 morphometric variables calculated for each group was tested using a Student's t-test. To apply t-tests, we have transformed
167 the morphometric variables to remove skewness by taking their natural logarithm. Correlation analysis has been used to
168 investigate the correlation between the selected morphometric attributes of alcoves and fans. We infer strong positive
169 correlations between variables if the correlation coefficient value is more than 0.7 and strong negative correlations if the value
170 is less than -0.7. Very strong positive correlation between variables is inferred if the correlation coefficient is ≥ 0.9 . Further,
171 we used canonical discriminant analysis (CDA) to determine morphometric variables that provide the most discrimination
172 between the groups of gullies. In CDA, functions are generated according to the number of groups, until a number equal to $n -$
173 1 functions is reached (n is the number of groups) (Conway et al., 2015). For the two groups of gullies in our study, there is
174 going to be a function for which there is a standardised canonical discriminant function coefficient associated with the
175 morphometric variable. The higher the magnitude of this coefficient for a particular morphometric variable, the higher the role
176 of that variable in separating the groups of gullies. Standardisation was done by dividing each value for a given variable by
177 the maximum value.

Deleted: At f

178 4 Results

179 4.1 Morphology of gully systems

180 Out of the 29 gullied craters analysed in this work, we have found that there are 24 craters influenced by LDM and VFFs. The
181 remaining 5 craters have gullies incised into the exposed underlying bedrock on the wall of the crater. Below we describe the
182 substrates identified in the studied craters and then compare the morphology of the gullies formed into those substrates.

183 ~~4 craters out of 24 craters (i.e. Raga, Roseau, unnamed crater in Newton basin and unnamed crater-1 in Terra Sirenum) have~~
184 ~~gullies that are only influenced by LDM. In these craters, we have found morphological evidence of LDM in the form of~~
185 ~~polygonized, smooth textured material on the pole-facing walls of the craters.~~ Morphological evidence of VFF is not evident
186 in these craters. In these craters, the gully-alcoves ~~and gully channels appear to have been incised into the polygonized LDM~~
187 ~~material,~~ and the gully-fan deposits are ~~mantled~~. A typical example of this can be found in the unnamed crater formed inside
188 the Newton basin (Fig. 4a). Roseau crater, in particular, contains a large number of gully systems whose alcoves and fans are

Deleted: We found morphological evidence of LDM in the form of polygonized, smooth textured material on the pole-facing walls of 4 craters namely

Deleted: both

Deleted: covered by a smooth drape of polygonized LDM material

Deleted: pre-existing

197 extensively mantled (Fig. 4b). The remaining 20 out of 24 craters contain evidence for gullies that are influenced by both LDM
198 and glacial deposits (Table 1). The base of the pole-facing walls and the floor of the craters within which the gully systems
199 have formed host linear-to-sinuuous arcuate ridges and VFFs, respectively. Typical examples of VFFs can be found in Corozal,
200 Talu, unnamed craters in Terra Sirenum and Argyre basin, Langtang, Dechu and Dunkassa craters (Fig. 4c). In majority of the
201 gullied craters (except Raga, Roseau and unnamed crater-1 in Terra Sirenum) influenced by LDM and glacial deposits, gully
202 alcoves, are found to have a distinctive V-shaped cross section in their mid-section (Figures 4d and 4e), they do not extend up

Deleted: Additionally, younger generation of gullies are visible that have incised within the LDM.

Deleted: specifically incised LDM as opposed to LDM that infills pre-existing alcoves and gullies, and

Deleted: VFFs

Deleted: Gullies

Deleted: incised into LDM/VFFs

210 to the crater rim, and gully systems often show multiple episodes of activity, inferred by the presence of fresh channel incision
211 on the gully-fan surfaces (Fig. 4d-e).

212 Istok, Galap, Gasa, Los, and an unnamed crater in the Terra Sirenum contain gully systems on the pole-facing walls that are
213 not associated with LDM and VFFs (Table 1). The alcoves inside these craters have a crenulated shape and appear to have
214 formed by headward erosion into the bedrock of the crater rim (Fig. 4f). These craters have formed large gully systems on
215 their pole-facing walls, with brecciated alcoves, comprising of multiple sub-alcoves and hosting many clasts/boulders (Fig.
216 4f).

217

218

219

220

221

222

223

224

225

226

227

228

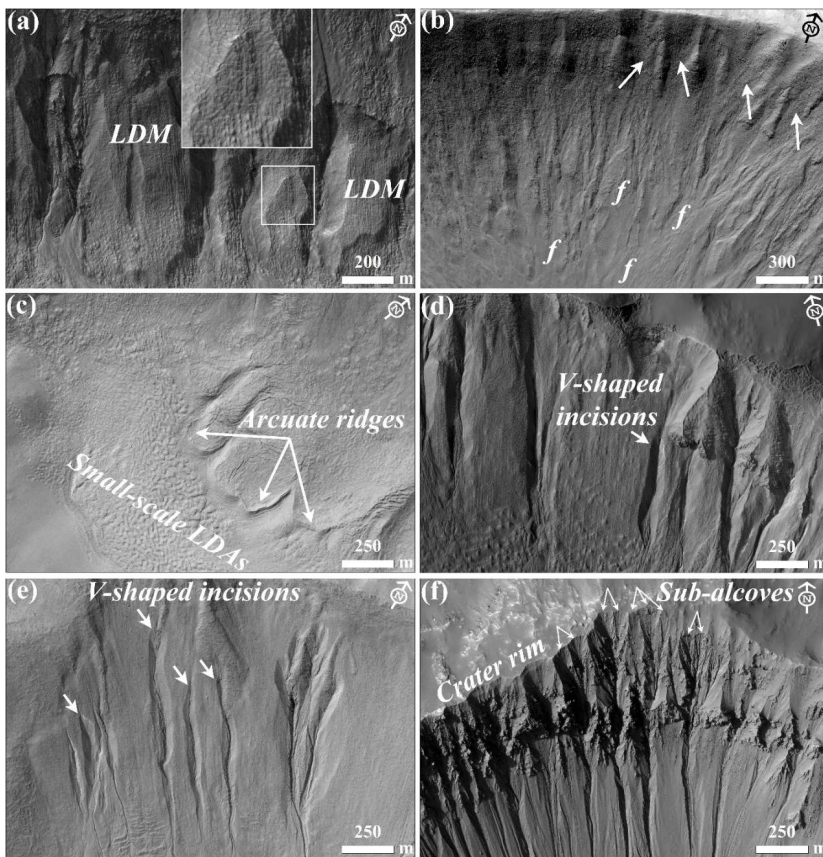
229

230

231

232

233



234 **Figure 4: (a) LDM draped on the wall of an unnamed crater in the Newton basin. The inset shows details of the polygonal texture of**
235 **the LDM. (HiRISE image PSP_002686_1410). (b) Infilled alcoves (arrows) and mantled fan surfaces (marked by letter 'f') on the**
236 **wall of Roseau crater. (HiRISE image ESP_024115_1380). (c) Arcuate ridges at the foot of the crater wall and small-scale LDAs on**
237 **the floor in Langtang crater. (HiRISE image ESP_030099_1415). (d) V-shaped incisions on the LDM draped walls of Taltal (HiRISE**
238 **image ESP_037074_1400) and (e) Langtang crater (HiRISE image ESP_030099_1415). (f) Alcoves formed in Los crater by headward**
239 **erosion into the crater rim. Individual alcoves formed in bedrock have multiple sub-alcoves. (HiRISE image ESP_020774_1445).**

240

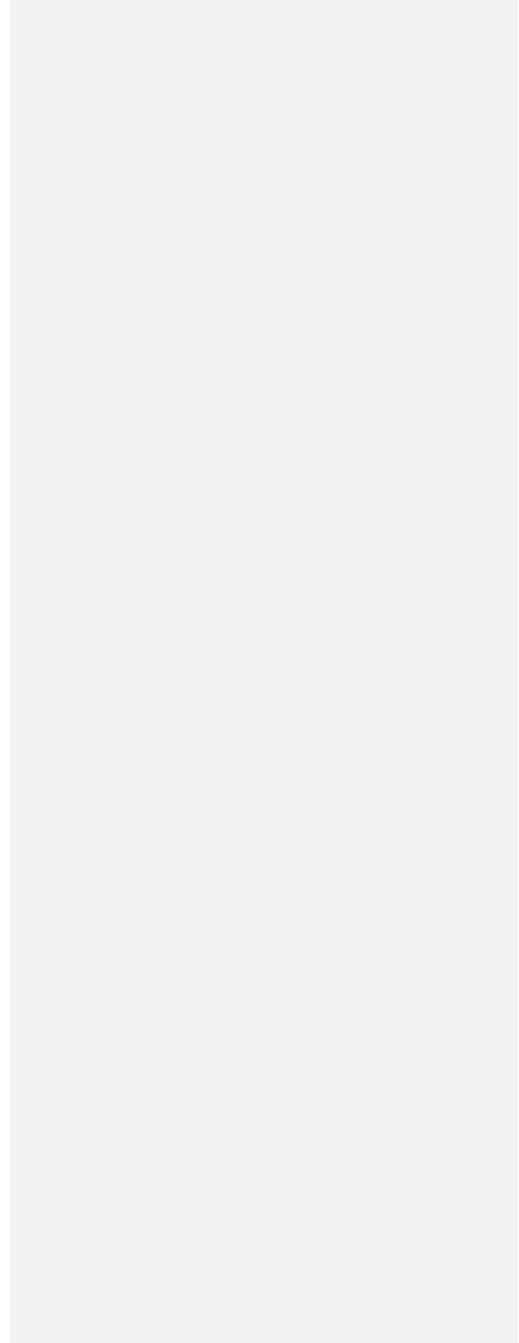
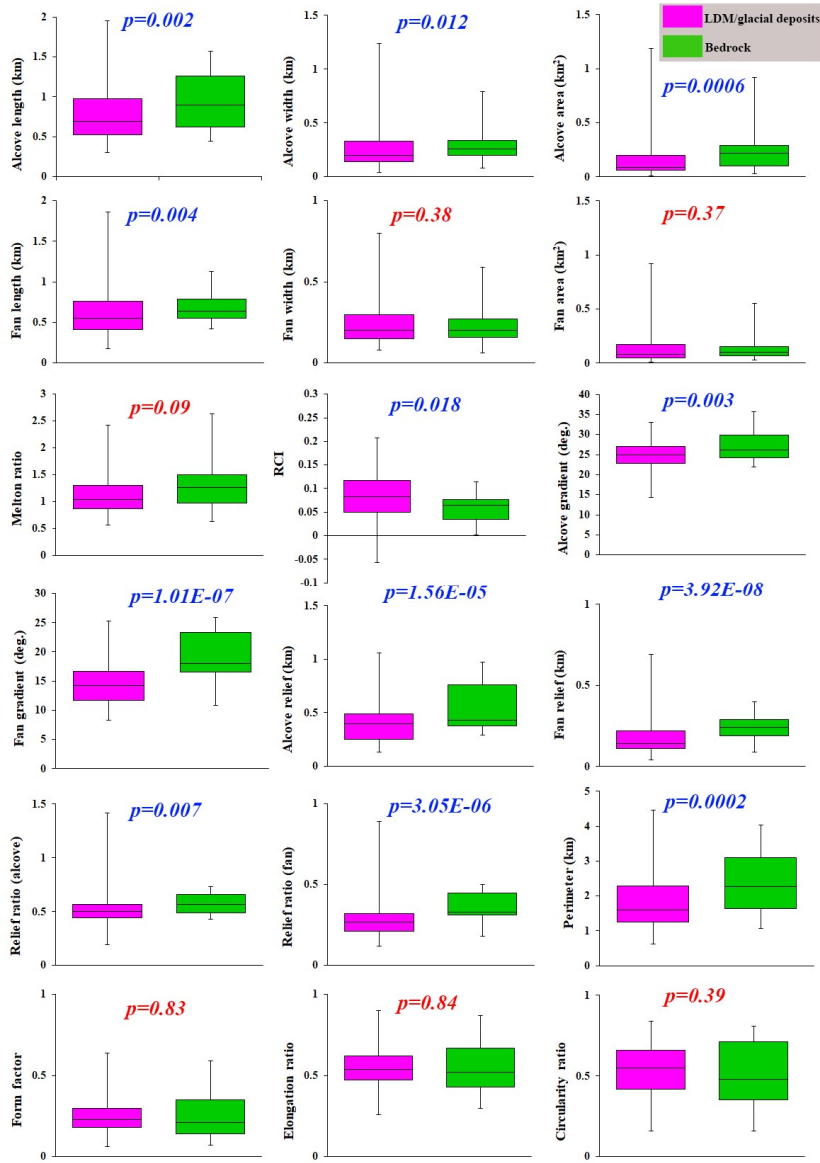
241 4.2 Morphometry of gully systems

242 Based on the criteria summarized in section 3.3, we have studied 167 gullies across 29 craters for calculation of morphometric
243 variables. 130 gullies are formed within LDM/glacial deposits, and 37 gullies are formed within the bedrock. The results of
244 morphometric calculations are summarized for visual comparison as a boxplot (Fig. 5).

245 The results of the Student's t-test indicates that all of the morphometric variables in Table 2, except fan width, fan area, Melton
246 ratio, form factor, elongation ratio, and circularity ratio, differ significantly between LDM/glacial deposits and bedrock (Fig.
247 5). Compared to the mean gradient of gully-fans formed in LDM/glacial deposits, bedrock gully-fans are steeper and possess
248 a higher relief ratio. The interquartile range of length, relief, and perimeter of alcoves formed in bedrock are also higher than
249 the interquartile range of similar variables in LDM/glacial deposits, but the alcoves in LDM/glacial deposits possess much
250 higher values of length, relief, and perimeter (Fig. 5).

251

Deleted: melton

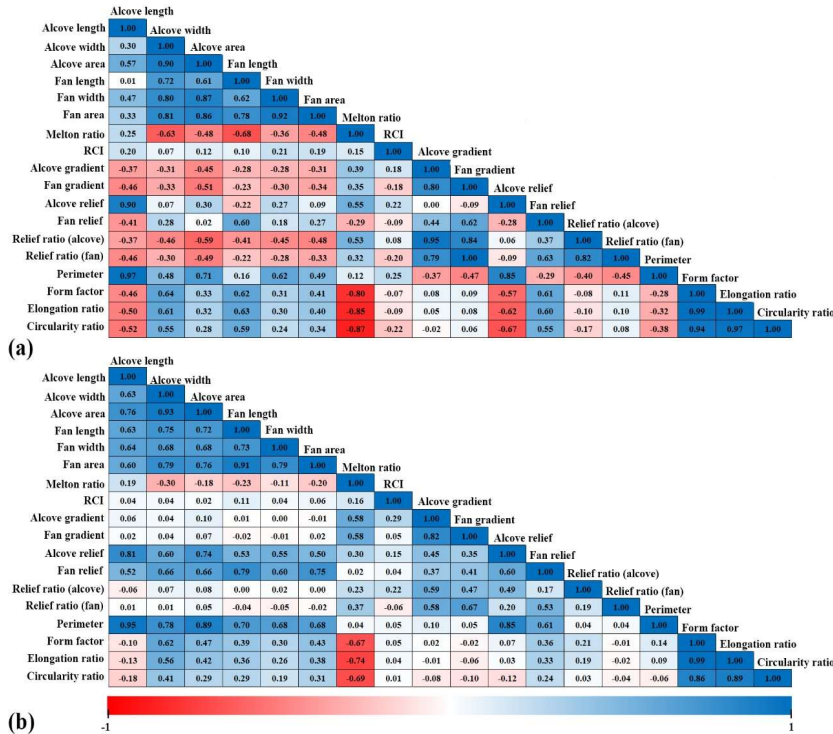


255 **Figure 5: Boxplots showing the range of values of alcove/fan geometry, relief, gradient, and dimensionless variables of gullies incised**
 256 **into LDM/glacial deposits (pink) and bedrock (green).** P-values on the plots represent the results of the student's t-tests for testing
 257 **the significance of difference in means of the morphometric variables between gully systems formed on LDM/Glacial deposits and**
 258 **bedrock. P-values in blue correspond to significant difference (with respect to a p-value of 0.05) and those in red are non-significant.**

259

260 Correlations between morphometric attributes of alcoves and fans formed in bedrock and LDM/glacial deposits are
 261 summarized in Fig. 6. For bedrock, there are strong positive correlations between 12 pairs of morphometric variables and
 262 strong negative correlations between 3 pairs of morphometric variables. For LDM/glacial deposits, there are strong positive
 263 correlations between 18 pairs of morphometric variables and strong negative correlations between 3 pairs of morphometric
 264 variables. Very strong positive correlations are found between 9 pairs of morphometric variables for bedrock and between 4
 265 pairs of morphometric variables for LDM/glacial deposits.

266



267 **Figure 6: Correlations between morphometric attributes of alcoves and fans formed in (a) bedrock and (b) LDM/glacial deposits.**
268 **Higher the value of the correlation coefficient, higher is the strength of the correlation.**

269

270 The canonical discriminant analysis reveals that the following morphometric variables best distinguish between the gully
271 systems formed in LDM/glacial deposits and bedrock, in descending order of importance: alcove perimeter, alcove relief, fan
272 gradient, fan relief, fan length, relief ratio (alcove), alcove width, relief ratio (fan), alcove gradient, alcove area, alcove length,
273 and relative concavity index (Table 3). The alcove perimeter is most important in discriminating among the gully systems
274 formed within LDM/glacial deposits and bedrock, and the next two most important variables are alcove relief and fan gradient.
275 Alcove relief and fan gradient have 4/5 and 1/3 the weight of alcove perimeter, respectively. The remaining variables such as
276 fan relief, fan length, relief ratio (alcove), alcove width, and relief ratio (fan) have nearly 1/5 the weight of alcove perimeter
277 or greater (but less than 1/3) discriminatory power in separating between the gullies formed in LDM/glacial deposits and
278 bedrock. The variables with the smallest magnitude, alcove gradient, alcove area, alcove length and relative concavity index,
279 have less than 1/10 the weight of the most important variable in separating the gully systems.

280 **Table 3.** Standardised canonical discriminant function coefficients (F1) that best separate gully systems formed on
281 LDM/Glacial deposits and bedrock.

Variable	F1
Perimeter	3.552
Alcove relief	-2.828
Fan gradient	1.278
Fan length	-1.06
Fan relief	1.06
Relief ratio (alcove)	0.971
Alcove width	-0.692
Relief ratio (fan)	-0.665
Alcove gradient	-0.331
Alcove area	-0.319
Alcove length	0.23
Relative concavity index	-0.182

282

283 5 Discussions

284 5.1 Unique morphology and morphometry of gully systems in different substrates

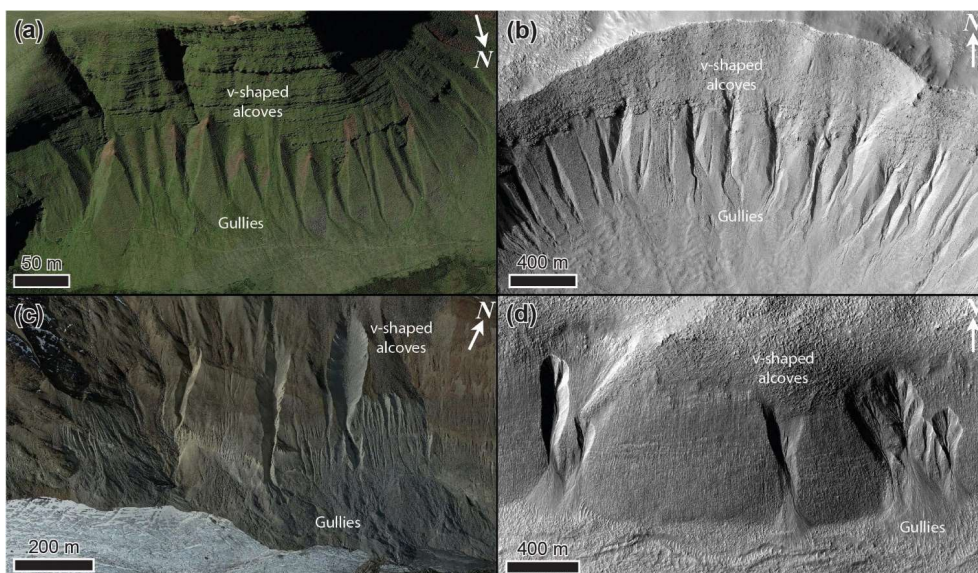
285 We have found that the gully systems formed in LDM/glacial deposits and bedrock can, using discriminatory analysis, be
286 distinguished from one another in terms of perimeter and relief of alcoves (Table 3). Additionally, we have found statistically
287 significant difference between the perimeter and relief of alcoves formed in LDM/glacial deposits and bedrock (Fig. 5). It is
288 likely that these differences in the perimeter and relief of alcoves formed within morphologically distinct substrates could be
289 due to the integral nature of the surface material within which the alcoves have formed. In other words, it is possible that the
290 differences in the physical properties of the sediments (~~namely~~ grain size, compactness etc.) within which alcoves have formed
291 played a key role in erosion of the substrate leading to differences in their morphometric variables. Below we elaborate on the
292 uniqueness of the substrates within which alcoves have formed, and discuss further the relationships between the morphometric
293 variables of the morphologically distinct gully systems.

294 On Mars, VFFs contain high purity glacial ice with a debris cover (Sharp, 1973; Squyres, 1978, 1979; Squyres and Carr, 1986;
295 Holt et al 2008, Plaut et al 2009, Petersen et al. 2018). Their surfaces have been interpreted to be comprised of finer, reworked
296 debris derived from sublimation of the underlying ice (Mangold, 2003; Levy et al., 2009a; Morgan et al., 2009). The smooth,
297 meters thick draping unit on the walls of formerly glaciated craters has been suggested to be derived from the atmosphere as a
298 layer of dust-rich ice primarily constituting of fine-grained materials (Kreslavsky and Head, 2000; Mustard et al., 2001). The
299 fine-grained materials are loosely-packed, unconsolidated materials exhibiting low thermal inertia values (Mellon et al., 2000;
300 Putzig et al., 2005). Typically, gullies formed within this substrate display a smooth surface texture, wherein, evidence of
301 individual clasts or meter-scale boulders is not resolvable in HiRISE images, substantiating the dominant component of fine-
302 grained materials within the LDM (e.g., Levy et al., 2010; de Haas et al., 2015a). Additionally, it has been found that alcoves
303 incised into the LDM always have a distinctive V-shaped cross section in their mid-section (Figures 4d and 4e), which when
304 compared with similar-scaled systems on Earth also corresponds to the presence of loose sediments constituting the LDM
305 (Conway et al., 2018). The alcoves with V-shaped cross sections are found to be elongated, likely indicating incision within
306 ice-rich unlithified sediments (Aston et al., 2011). In the studied craters, we have found that gullies incised into LDM/glacial
307 deposits are having an elongated, V-shaped cross section in their mid-section (Fig. 4). We propose that the presence of fine-
308 grained, loosely packed, unconsolidated materials within LDM/glacial deposits has facilitated formation of elongated alcoves
309 with perimeter and relief relatively higher than that of alcoves formed in coarse-grained bedrock substrate. This is consistent
310 with the previous studies suggesting that gullies eroding into LDM/glacial deposits have elongated catchments, whereas gullies
311 eroding into the bedrock have more amphitheater-shaped catchments (Levy et al., 2009b). For this reason, the estimated length
312 of alcoves formed in LDM/glacial deposits is found to be relative higher than that of alcoves formed in bedrock (Fig. 5).
313 Furthermore, statistical analysis has revealed a significant difference between the length of alcoves formed in LDM/glacial
314 deposits and bedrock (Fig. 5). Additionally, the presence of finer-grained sediments in LDM/glacial deposits is the likely cause

Deleted: viz.

316 of the V-shape of the incision of alcoves investigated in this study (Aston et al., 2011). On Earth, V-shaped incisions through
317 glacial ice-rich moraines have been observed to have occurred during the paraglacial phase of glacial retreat (Bennett et al.,
318 2000; Ewertowski and Tomczyk, 2015) (Fig. 7). The paraglacial phase refers to a terrestrial post-glacial period that represents
319 the response of changing environment to deglaciation (Bennett et al., 2000; Ewertowski and Tomczyk, 2015).

320



321

322 **Figure 7: Gullies forming in glacial sediments in deglaciated terrain in the (a) Brecon Beacons, Wales, UK on Earth (Google Earth**
323 **coordinates: 51°52'59.11"N, 3°43'33.26"W), (b) Talu crater (https://www.uahirise.org/ESP_011817_1395) on Mars, (c)**
324 **Hintereisferner, Austria (Google Earth coordinates: 46°48'54.25"N, 10°47'8.18"E), on Earth, and (d) Bunnik crater**
325 **(https://www.uahirise.org/ESP_047044_1420) on Mars. HiRISE image credit: NASA/JPL-Caltech/University of Arizona.**

326

327 The next most important difference between these two types of gullies is the mean gradient of gully fans. At the foot of the
328 fans, mean gradient of the fans influenced by LDM/glacial deposits is $<15^\circ$ for 61% of the studied fans. For bedrock, 84% of
329 the studied fans have a mean gradient $>15^\circ$ at the foot of the fans. Hence, gully-fans formed in bedrock are emplaced at a
330 relatively steeper gradient than the fans formed from gullies in LDM/glacial deposits. We propose that the nature of the material

331 mobilized can explain this difference, with the finer-grained sediments characteristic of the LDM/glacial type gullies being
332 easier to mobilise and being entrained to lower slope angles, than the coarser sediments found within the bedrock type gullies.

333 **5.2 Evaluation of the gully formation process**

334 On Earth, alcove-fan systems can roughly be subdivided in flood-dominated, debris-flow dominated, and colluvial systems.
335 Following the terminology of De Haas et al., (2015b) and Tomczyk (2021), we define these systems as follows:

336 1) Flood-dominated systems: These are systems dominated by fluid-gravity flows, i.e., water floods, hyperconcentrated floods,
337 and debris floods. The fans of such systems are commonly referred to as fluvial or alluvial fans (e.g., Ryder, 1971; Blair and
338 McPherson, 1994; Hartley et al., 2005).

339 2) Debris-flow dominated systems: These are systems dominated by sediment-gravity flows, i.e., debris flows, mud flows.
340 Irrespective of their radial extent and depositional gradients, the fans aggraded by these systems can be commonly called
341 debris-flow fans or debris fans (Blikra and Nemeč, 1998; de Scally et al., 2010).

342 3) Colluvial systems: These are systems dominated by rock-gravity and sediment-gravity flows, with their dominant activity
343 relating to rockfalls, grain flows, and snow avalanches (in periglacial and alpine settings). Debris flows typically constitute
344 only a relatively minor component of geomorphic processes in such systems. The fans of these systems are also commonly
345 known as colluvial cones or talus cones (Siewert et al., 2012; De Haas et al., 2015b).

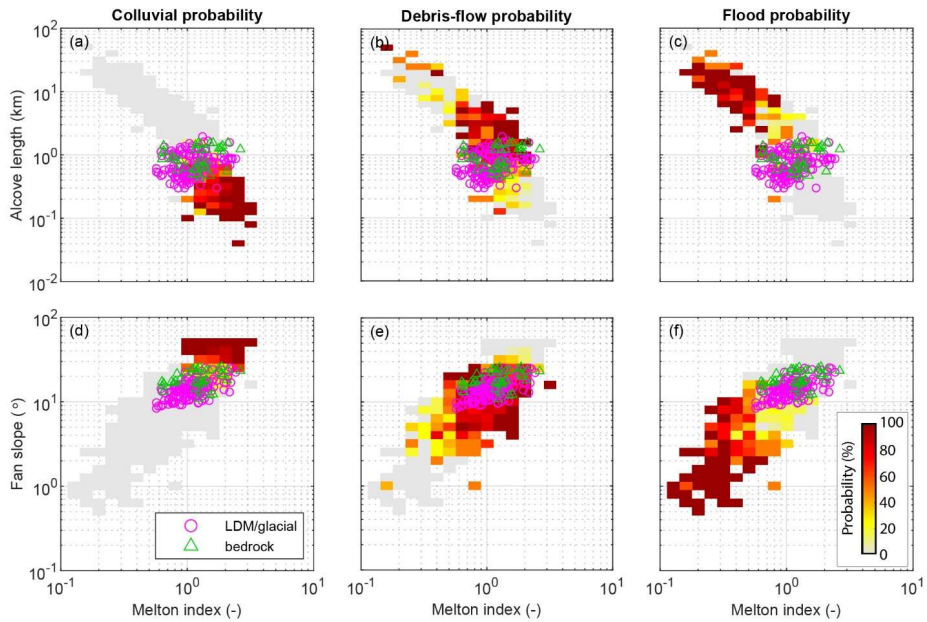
346 Although these systems may be dominated by one type of geomorphic process, it is important to stress that other processes
347 may also occur. For example, on Earth water floods are not uncommon on many debris-flow dominated systems, while debris-
348 flow deposits are commonly recognized on colluvial cones.

349

350

351

352



353

354 **Figure 8: Comparison of combinations of Melton ratio with Alcove length and Fan gradient. The probability heat maps**
355 **are based on previously published data – see text for references. The Martian gully systems formed in LDM/glacial**
356 **deposits and bedrock are found to be in the debris-flow regime on Earth. The gray area shows the realm of the colluvial,**
357 **debris-flow, and fluvial fans together.**

358

359 To compare the morphometric characteristics of the Martian gully systems to terrestrial systems, we have compiled
360 morphometric data of alcoves and fans across several continents, mountain ranges, climate zones, and process types on Earth.
361 This dataset includes published data from the Himalayas, Ladakh, India (Stolle et al., 2013), the tropical Andes, Columbia
362 (Arango et al., 2021), Spitsbergen, Svalbard (Tomczyk, 2021), British Columbia, Canada (Kostaschuk, 1986; Jackson et al.,
363 1987; and newly presented data), the southern Carpathians, Romania (Ilinca et al., 2021), the Southern Alps, New Zealand (De
364 Scally and Owens, 2004; De Scally et al., 2010), the North Cascade Foothills, USA, the European Alps (including Switzerland,
365 Italy, France, and Austria), and the Pyrenees (from multiple authors compiled by Bertrand et al., 2013). The dataset comprises
366 information from colluvial, debris-flow, and flood (also including debris flood) dominated systems. In total, it contains 231

367 colluvial systems, 749 debris-flow dominated systems, and 369 flood-dominated systems. In total, data were compiled for
368 1349 systems, although not all information was available for all systems, with data availability ranging from 729 sites for
369 alcove length to all 1349 systems for Melton index and process type. Based on this data we have made a heatmap of the
370 probability of flood, debris-flow, or colluvially-dominated conditions for combinations of Melton ratio with alcove length and
371 fan gradient, to which we compare the Martian gullies (Fig. 8). We have specifically chosen the combinations of Melton ratio
372 with alcove length and fan gradient to infer the Martian gully formative mechanism because they have been widely used in
373 discriminating terrestrial drainage basins and fans prone to flooding from those subject to debris flows, debris floods and floods
374 (e.g. De Scally and Owens, 2004; Wilford et al., 2004). We have found that the Martian gullies are indeed in the debris-flow
375 regime on Earth. Moreover, they are closer to the transition to the smaller and steeper colluvial cones than to transition to
376 flood-dominated fans. As expected, bedrock systems in Fig. 8d-e are closer to the colluvial systems than the LDM systems.

377

378 According to the previous reports of debris-flow like deposits found in Martian gullies (e.g. Johnsson et al., 2014; Sinha et al.,
379 2019, 2020), the morphological attributes of debris-flow like deposits typically include overlapping tongue-shaped lobes with
380 embedded clasts, channels with medial deposits, and channels with clearly defined lateral levees. Although it is still not clear
381 whether the formation of these deposits in gullies are from sublimation of CO₂ ice or due to meltwater generation. De Haas et
382 al., (2019b) showed that CO₂ sublimation may lead to flow fluidization on Mars in a manner similar to fluidization by water
383 in terrestrial debris flows; a concept supported by the recent finding of lobate deposits and boulder-rich levee formation during
384 the present-day in Istok crater (Table 1) (Dundas et al., 2019). The formation of these morphologically similar deposits during
385 the present-day is attributed to sublimating CO₂ frost, which likely produces the necessary fluidization likely by gas generated
386 from entrained CO₂ frost (Dundas et al., 2019). On the basis of these recent reports (De Haas et al., 2019b; Dundas et al., 2019)
387 and based on our own findings in this study, we argue that a debris-flow like process similar to those operated in the terrestrial
388 gully systems has likely dominated the flow types that lead to gully formation on Mars. It is likely that the present-day
389 sublimation of CO₂ ice on Mars provided the necessary flow fluidization for the emplacement of deposits similar to terrestrial
390 debris-flow like deposits (De Haas et al., 2019b).

391 6 Conclusions

392 This paper compares morphological and morphometric characteristics of gully alcoves and associated fans formed in
393 LDM/glacial deposits and bedrock over walls of 29 craters between 30° S and 75° S latitudes. 5 craters out of 29 have alcoves-
394 fans formed within the bedrock and remaining 24 craters have alcoves-fans formed within LDM/glacial deposits. From our
395 analysis of 167 gullies, we posit that gully systems formed in LDM/glacial deposits and bedrock differ from one another using
396 the following lines of evidence:

Formatted: Font: Not Bold

Formatted: Font: Not Bold

397 • Alcoves formed in LDM/glacial deposits are more elongated than the alcoves formed in bedrock, and possess a distinctive
398 V-shaped cross section.

399 • The mean gradient of gully-fans formed in bedrock is steeper than the mean gradient of fans formed from gullies in
400 LDM/glacial deposits.

401 The morphological distinction reported between gullies formed in the bedrock and LDM/glacial deposits signifies that Martian
402 gullies may have multiple formative mechanisms. We infer that the presence of mantling material could be one of the key
403 factors in constraining the mechanisms forming Martian gully systems and that presence of LDM would promote formation
404 of elongated alcoves with perimeter and relief relatively higher than that of alcoves formed in coarse-grained bedrock substrate.

405 Based on the combinations of Melton ratio with alcove length and fan gradient, we suggest that the gully systems studied in
406 this work were likely dominated by terrestrial debris-flow like processes during their formation. This is consistent with the
407 findings reported in previous studies that showed evidence of formation of deposits morphologically similar to terrestrial
408 debris-flow like deposits, both in the past and during the present-day (e.g., Johnsson et al., 2014; Dundas et al., 2019). The
409 present-day sublimation of CO₂ ice on Mars is envisaged to provide the necessary flow fluidization for the emplacement of
410 deposits similar to debris-flow like deposits on Earth (De Haas et al., 2019b).

411 **7 Author contribution**

412 RKS, TDH and SJC conceptualized this work. The methodology was developed by RKS, TDH and SJC. Data curation and
413 formal analyses were performed by RKS. TDH and AN also contributed in collection of datasets used in this work. RKS, DR,
414 TDH and SJC contributed to the interpretation of the data and results. RKS wrote the original draft of this paper, which was
415 reviewed and edited by all authors.

416 **8 Conflict of interest**

417 SJC is a Guest Editor of this special issue (Planetary landscapes, landforms, and their analogues) of ESurfD and on the editorial
418 board for ESurf. The peer-review process was guided by an independent editor, and the authors have also no other competing
419 interests to declare.

420 **9 Acknowledgements**

421 We are grateful and thank both the anonymous reviewers for thorough assessment of our manuscript and for providing us
422 constructive comments and suggestions. Thanks to the Editor (Heather Viles) and Associate Editor (Frances E. G. Butcher) at
423 Earth Surface Dynamics for the editorial handling of the manuscript. We would like to thank the HiRISE team for their work
424 to produce the images and digital elevation models used in this study, it would have been impossible without them. RKS and
425 DR acknowledge the financial support by the Indian Space Research Organisation, Department of Space, Government of India.

426 SJC and AN are grateful for the financial support from Région Pays de la Loire, project étoiles montantes METAFLOWS
427 (convention N° 2019-14294) and also the financial support of CNES in support of their HiRISE work. TdH was supported by
428 the Netherlands Organisation for Scientific Research (NWO) (grant 016.Veni.192.001). We acknowledge the efforts of team
429 MUTED to develop an online tool (<http://muted.wwu.de/>) for quick identification of the spatial and multi-temporal coverage
430 of planetary image data from Mars. All the planetary datasets used in this work are available for free download at the PDS
431 Geosciences Node Mars Orbital Data Explorer (ODE) (<https://ode.rsl.wustl.edu/mars/>) and <https://www.uahirise.org/>. The
432 newly-generated DTMs can be downloaded from https://figshare.com/articles/dataset/Self_generated_DEMs/21717164.
433 The measurement datasets can be downloaded from
434 [https://figshare.com/articles/dataset/Measurement_data_of_gully_systems_in_the_southern_mid_latitudes_of_Mars/](https://figshare.com/articles/dataset/Measurement_data_of_gully_systems_in_the_southern_mid_latitudes_of_Mars/21717182)
435 [21717182](https://figshare.com/articles/dataset/Measurement_data_of_gully_systems_in_the_southern_mid_latitudes_of_Mars/21717182). This work is a part of the PhD work of Rishitosh K. Sinha. Director PRL, Head of Planetary Science Division,
436 PRL, Head of Planetary Remote Sensing Section, PRL, and Director IIT Gandhinagar are gratefully acknowledged for constant
437 encouragement during the work.

438 **References**

- 439 Arango, M. I., Aristizábal, E., & Gómez, F.: Morphometrical analysis of torrential flows-prone catchments in tropical and
440 mountainous terrain of the Colombian Andes by machine learning techniques, *Natural Hazards*, 105(1), 983-1012, doi:
441 <https://doi.org/10.1007/s11069-020-04346-5>, 2021.
- 442 Arfstrom, J. & Hartmann, W.K.: Martian flow features, moraine-like ridges, and gullies: terrestrial analogs and
443 interrelationships, *Icarus*, 174, 321-335, doi: <https://doi.org/10.1016/j.icarus.2004.05.026>, 2005.
- 444 Aston, A., Conway, S. & Balme, M.: Identifying Martian Gully Evolution. In: Balme, M.R., Bargery, A.S., Gallagher, C.J. &
445 Gupta, S. (eds) *Martian Geomorphology*, Geological Society, London, Special Publications, 356, 151-169, doi:
446 <https://doi.org/10.1144/SP356.9>, 2011.
- 447 Balme, M., Mangold, N. Et Al.: Orientation and distribution of recent gullies in the southern hemisphere of Mars: observations
448 from High Resolution Stereo Camera/Mars Express (HRSC/MEX) and Mars Orbiter Camera/Mars Global Surveyor
449 (MOC/MGS) data, *J. Geophys. Res.: Planets*, 111, E05001, doi: <https://doi.org/10.1029/2005JE002607>, 2006.
- 450 Bertrand, M., Liébault, F., & Piégay, H.: Debris-flow susceptibility of upland catchments, *Natural Hazards*, 67(2), 497-511,
451 doi: <https://doi.org/10.1007/s11069-013-0575-4>, 2013.
- 452 Blair, T.C. & McPherson, J.G.: Processes and forms of alluvial fans. In: PARSONS, A. & ABRAHAMS, A. (eds)
453 *Geomorphology of Desert Environments*, Springer, Dordrecht, The Netherlands, 413-467, doi: [https://doi.org/10.1007/978-1-](https://doi.org/10.1007/978-1-4020-5719-9_14)
454 [4020-5719-9_14](https://doi.org/10.1007/978-1-4020-5719-9_14), 2009.

455 Blair, T.C.: Sedimentology of the debris-flow-dominated Warm Spring Canyon alluvial fan, Death Valley, California,
456 *Sedimentology* 46 (5), 941–965, doi: <https://doi.org/10.1046/j.1365-3091.1999.00260.x>, 1999.

457 Blikra, L.H., Nemeč, W.: Postglacial colluvium in western Norway: depositional processes, facies and palaeoclimatic record.
458 *Sedimentology* 45 (5), 909–960, doi: <https://doi.org/10.1046/j.1365-3091.1998.00200.x>, 1998.

459 Cedillo-Flores, Y., Treiman, A.H., Lasue, J. & Clifford, S.M.: CO₂ gas fluidization in the initiation and formation of Martian
460 polar gullies, *Geophys. Res. Letters*, 38, L21202 doi: <https://doi.org/10.1029/2011GL049403>, 2011.

461 Christensen, P.R.: Formation of recent Martian gullies through melting of extensive water-rich snow deposits, *Nature*, 422,
462 45–48, doi: <https://doi.org/10.1038/nature01436>, 2003.

463 Conway, S. J., Butcher, F. E., de Haas, T., Deijns, A. A., Grindrod, P. M., & Davis, J. M.: Glacial and gully erosion on Mars:
464 A terrestrial perspective, *Geomorphology*, 318, 26-57, doi: <https://doi.org/10.1016/j.geomorph.2018.05.019>, 2018.

465 Conway, S.J. & Balme, M.R.: Decameter thick remnant glacial ice deposits on Mars, *Geophys. Res. Letters*, 41, 5402–5409,
466 doi: <https://doi.org/10.1002/2014GL060314>, 2014.

467 Conway, S.J., Balme, M.R., Kreslavsky, M.A., Murray, J.B. & Towner, M.C.: The comparison of topographic long profiles
468 of gullies on Earth to gullies on Mars: a signal of water on Mars. *Icarus*, 253, 189–204, doi:
469 <https://doi.org/10.1016/j.icarus.2015.03.009>, 2015.

470 Conway, S.J., Balme, M.R., Murray, J.B., Towner, M.C., Okubo, C.H. & Grindrod, P.M.: The indication of Martian gully
471 formation processes by slope–area analysis, In: Balme, M.R., Bargery, A.S., Gallagher, C.J. & Gupta, S. (eds) *Martian*
472 *Geomorphology*, Geological Society, London, Special Publications, 356, 171–201, doi: <https://doi.org/10.1144/SP356.10>,
473 2011.

474 Conway, S.J., Harrison, T.N., Soare, R.J., Britton, A.W. & Steele, L.J.: New slope-normalized global gully density and
475 orientation maps for Mars, In: Conway, S.J., Carrivick, J.L., Carling, P.A., De Haas, T. & Harrison, T.N. (eds) *Martian Gullies*
476 *and their Earth Analogues*, *Geol. Soc. Lond. Spec. Publ.* 467. First published online November 27, 2017, doi:
477 <https://doi.org/10.1144/SP467.3>, 2017.

478 Costard, F., Forget, F., Mangold, N. & Peulvast, J.P.: Formation of recent Martian debris flows by melting of near-surface
479 ground ice at high obliquity, *Science*, 295, 110–113, doi: [10.1126/science.1066](https://doi.org/10.1126/science.1066), 2002.

480 Crosta, G.B., Frattini, P.: Controls on modern alluvial fan processes in the central Alps, northern Italy, *Earth Surf. Proc. Land*.
481 29 (3), 267–293, doi: <https://doi.org/10.1002/esp.1009>, 2004.

482 de Haas, T., Conway, S.J., Butcher, F.E.G., Levy, J.S., Grindrod, P.M., Balme, M.R., Goudge, T.A.: Time will tell: temporal
483 evolution of Martian gullies and paleoclimatic implications, *Geol. Soc. Lond. Spec. Publ.* 467, doi:
484 <https://doi.org/10.1144/SP467.1>, 2019a.

485 de Haas, T., McArdell, B. W., Conway, S. J., McElwaine, J. N., Kleinhans, M. G., Salese, F., & Grindrod, P. M.: Initiation
486 and flow conditions of contemporary flows in Martian gullies, *J. Geophys. Res.: Planets*, 124(8), 2246-2271, doi:
487 <https://doi.org/10.1029/2018JE005899>, 2019b.

488 de Haas, T., Hauber, E. & Kleinhans, M.G. 2013. Local late Amazonian boulder breakdown and denudation rate on Mars,
489 *Geophys. Res. Letters*, 40, 3527–3531, doi: <https://doi.org/10.1002/grl.50726>, 2013.

490 de Haas, T., Ventra, D., Hauber, E., Conway, S.J. & Kleinhans, M.G.: Sedimentological analyses of Martian gullies: the
491 subsurface as the key to the surface, *Icarus*, 258, 92–108, doi: <https://doi.org/10.1016/j.icarus.2015.06.017>, 2015a.

492 de Haas, T., Kleinhans, M. G., Carbonneau, P. E., Rubensdotter, L., & Hauber, E.: Surface morphology of fans in the high-
493 Arctic periglacial environment of Svalbard: Controls and processes, *Earth-Science Reviews*, 146, 163-182, doi:
494 <https://doi.org/10.1016/j.earscirev.2015.04.004>, 2015b.

495 de Scally, F. A., & Owens, I. F.: Morphometric controls and geomorphic responses on fans in the Southern Alps, New Zealand,
496 *Earth Surface Processes and Landforms: The Journal of the British Geomorphological Research Group*, 29(3), 311-322, doi:
497 <https://doi.org/10.1002/esp.1022>, 2004.

498 De Scally, F.A., Owens, I.F., Louis, J.: Controls on fan depositional processes in the schist ranges of the Southern Alps, New
499 Zealand, and implications for debris-flow hazard assessment, *Geomorphology* 122 (1–2), 99–116, doi:
500 <https://doi.org/10.1016/j.geomorph.2010.06.002>, 2010.

501 Dickson, J.L. & Head, J.W.: The formation and evolution of youthful gullies on Mars: gullies as the latestage phase of Mars
502 most recent ice age, *Icarus*, 204, 63–86, doi: <https://doi.org/10.1016/j.icarus.2009.06.018>, 2009.

503 Dickson, J.L. et al.: Recent climate cycles on Mars: Stratigraphic relationships between multiple generations of gullies and the
504 latitude dependent mantle, *Icarus* 252, 83–94, doi: <http://dx.doi.org/10.1016/j.icarus.2014.12.035>, 2015.

505 Dickson, J.L., Head, J.W., Fassett, C.I.: Patterns of accumulation and flow of ice in the mid-latitudes of Mars during the
506 Amazonian, *Icarus* 219, 723–732, doi: <http://dx.doi.org/10.1016/j.icarus.2012.03.010>, 2012.

507 Dickson, J.L., Head, J.W., Kreslavsky, M.: Martian gullies in the southern midlatitudes of Mars: Evidence for climate-
508 controlled formation of young fluvial features based upon local and global topography, *Icarus* 188, 315–323, doi:
509 <https://doi.org/10.1016/j.icarus.2006.11.020>, 2007.

510 Dundas, C. M., McEwen, A. S., Diniega, S., Hansen, C. J., Byrne, S., & McElwaine, J. N.: The formation of gullies on Mars
511 today, *Geol. Soc. Lond. Spec. Publ.* 467, 67-94, doi: <https://doi.org/10.1144/SP46>, 2019.

512 Dundas, C.M., Diniega, S., Hansen, C.J., Byrne, S., McEwen, A.S.: Seasonal activity and morphological changes in martian
513 gullies, *Icarus* 220:124–143, doi: <https://doi.org/10.1016/j.icarus.2012.04.005>, 2012.

514 Dundas, C.M., Diniega, S., McEwen, A.S.: Long-term monitoring of Martian gully formation and evolution with
515 MRO/HiRISE, *Icarus* 251:244–263, doi: <https://doi.org/10.1016/j.icarus.2014.05.013>, 2015.

516 [Hargitai, H. \(2014\). Viscous Flow Features \(Mars\). In: Encyclopedia of Planetary Landforms. Springer, New York, NY.](https://doi.org/10.1007/978-1-4614-9213-9_596-1)
517 https://doi.org/10.1007/978-1-4614-9213-9_596-1

518 Harrison, T.N., Osinski, G.R., Tornabene, L.L., Jones, E.: Global documentation of gullies with the Mars reconnaissance
519 orbiter context camera and implications for their formation, *Icarus* 252:236–254, doi:
520 <https://doi.org/10.1016/j.icarus.2015.01.022>, 2015.

521 Hartley, A.J., Mather, A.E., Jolley, E., Turner, P.: Climatic controls on alluvial-fan activity, Coastal Cordillera, northern Chile.
522 In: Harvey, A.M., Mather, A.E., Stokes, M. (Eds.), *Alluvial Fans: Geomorphology, Sedimentology, Dynamics*. *Geol. Soc.*
523 *Lond. Spec. Publ.* 251, 95-115, doi: <https://doi.org/10.1144/GSL.SP.2005.251.01>, 2005.

524 Head, J.W., Marchant, D.R., Dickson, J.L., Kress, A.M., Baker, D.M.: Northern midlatitude glaciation in the Late Amazonian
525 period of Mars: criteria for the recognition of debris-covered glacier and valley glacier landsystem deposits, *Earth Planet. Sci.*
526 *Lett.* 294:306–320, doi: <https://doi.org/10.1016/j.epsl.2009.06.041>, 2010.

527 HELDMANN, J.L. & MELLON, M.T.: Observations of Martian gullies and constraints on potential formation mechanisms,
528 *Icarus*, 168, 285–304, doi: <https://doi.org/10.1016/j.icarus.2003.11.024>, 2004.

529 Heldmann, J.L. et al.: Formation of martian gullies by the action of liquid water flowing under current martian environmental
530 conditions, *J. Geophys. Res. Planets* 110, doi: <http://dx.doi.org/10.1029/2004JE002261>, 2005.

531 Hobbs, S.W., Paull, D.J., Clark, J.D.A.: A comparison of semiarid and subhumid terrestrial gullies with gullies on Mars:
532 Implications for martian gully erosion, *Geomorphology* 204, 344–365, doi: <http://dx.doi.org/10.1016/j.geomorph.2013.08.018>,
533 2014.

534 Hobbs, S.W., Paull, D.J. and Clarke, J.D.A.: Analysis of regional gullies within Noachis Terra, Mars: A complex relationship
535 between slope, surface material and aspect, *Icarus*, 250, 308-331, doi: <https://doi.org/10.1016/j.icarus.2014.12.011>, 2015.

536 Hubbard, B., Milliken, R.E., Kargel, J.S., Limaye, A. & Souness, C.: Geomorphological characterisation and interpretation of
537 a mid-latitude glacier-like form: Hellas Planitia, Mars, *Icarus*, 211, 330–346, doi: <https://doi.org/10.1016/j.icarus.2010.10.021>,
538 2011.

539 Ilinca, V.: Using morphometrics to distinguish between debris flow, debris flood and flood (Southern Carpathians, Romania),
540 *Catena*, 197, 104982, doi: <https://doi.org/10.1016/j.catena.2020.104982>, 2021.

541 Jackson LE, Kostaschuk RA, MacDonald GM: Identification of debris flow hazard on alluvial fans in the Canadian Rocky
542 Mountains, In: Costa JE, Wieczorek GF (eds) *Debris flows/avalanches: process, recognition, and mitigation*. *Rev Eng Geol*
543 vol. VII. *Geol. Soc. Am*, doi: <https://doi.org/10.1130/REG7-p115>, 1987.

544 Johnsson, A. et al.: Evidence for very recent melt-water and debris flow activity in gullies in a young mid-latitude crater on
545 Mars, *Icarus* 235, 37–54, doi: <http://dx.doi.org/10.1016/j.icarus.2014.03.005>, 2014.

546 Kirk, R.L., Howington-Kraus, E., Rosiek, M.R., Anderson, J.A., Archinal, B.A., Becker, K.J., Cook, D.A., Galuszka, D.M.,
547 Geissler, P.E., Hare, T.M., Holmberg, I.M., Keszthelyi, L.P., Redding, B.L., Delamere, W.A., Gallagher, D., Chapel, J.D.,
548 Eliason, E.M., King, R., McEwen, A.S.: Ultrahigh resolution topographic mapping of Mars with MRO HiRISE stereo images:
549 meter-scale slopes of candidate Phoenix landing sites, *J. Geophys. Res. Planets* 113, doi:
550 <https://doi.org/10.1029/2007JE003000>, 2008.

551 Kostaschuk, R.A., Macdonald, G.M., Putnam, P.E.: Depositional process and alluvial fan-drainage basin morphometric
552 relationships near Banff, Alberta, Canada, *Earth Surf. Proc. Land.* 11 (5), 471–484, doi:
553 <https://doi.org/10.1002/esp.3290110502>, 1986.

554 Kreslavsky, M.A.: Slope steepness of channels and aprons: Implications for origin of martian gullies. Workshop Martian
555 Gullies, Workshop on Martian Gullies 2008. Abs.#1301, 2008.

556 Kreslavsky, M.A., Head, J.W.: Mars: nature and evolution of young latitudedependent water-ice-rich mantle, *Geophys. Res.*
557 *Lett.* 29, doi: <https://doi.org/10.1029/2002GL015392>, 2002.

558 Langbein, W. B.: Profiles of rivers of uniform discharge, *U.S. Geol. Surv. Prof. Pap.*, 501-B, 119– 122, doi:
559 <https://doi.org/10.1086/627653>, 1964.

560 Lanza, N. L., Meyer, G. A., Okubo, C. H., Newsom, H. E., & Wiens, R. C.: Evidence for debris flow gully formation initiated
561 by shallow subsurface water on Mars, *Icarus*, 205(1), 103-112, doi: <https://doi.org/10.1016/j.icarus.2009.04.014>, 2010.

562 Levy, J.S. et al.: Identification of gully debris flow deposits in Protonilus Mensae, Mars: Characterization of a water-bearing,
563 energetic gully-forming process, *Earth Planet. Sci. Lett. Mars Express after 6 Years in Orbit: Mars Geology from Three-*
564 *Dimensional Mapping by the High Resolution Stereo Camera (HRSC) Experiment 294*, 368–377, doi:
565 <https://doi.org/10.1016/j.epsl.2009.08.002>, 2010b.

566 Levy, J.S., Head, J., Marchant, D.: Thermal contraction crack polygons on Mars: classification, distribution, and climate
567 implications from HiRISE observations, *J. Geophys. Res. Planets* 114, 01007, doi: <https://doi.org/10.1029/2008JE003273>,
568 2009a.

569 Levy, J. S., Head, J. W., Marchant, D. R., Dickson, J. L., & Morgan, G. A.: Geologically recent gully–polygon relationships
570 on Mars: Insights from the Antarctic Dry Valleys on the roles of permafrost, microclimates, and water sources for surface
571 flow, *Icarus*, 201(1), 113-126, doi: <https://doi.org/10.1016/j.icarus.2008.12.043>, 2009b.

572 Levy, J.S., Head, J.W., Marchant, D.R.: Gullies, polygons and mantles in Martian permafrost environments: cold desert
573 landforms and sedimentary processes during recent Martian geological history, *Geol. Soc. Lond. Spec. Publ.* 354, 167–182,
574 doi: <https://doi.org/10.1144/SP354.10>, 2011.

575 Malin, M.C., Edgett, K.S.: Evidence for recent groundwater seepage and surface runoff on Mars. *Science* 288:2330–2335, doi:
576 <https://doi.org/10.1126/science.288.5475.2330>, 2000.

577 Mcewen, A.S., Eliason, E.M. et al.: Mars reconnaissance orbiter’s High Resolution Imaging Science Experiment (HiRISE), *J.*
578 *Geophys. Res.: Planets*, 112, E05S02, doi: <https://doi.org/10.1029/2005JE002605>, 2007.

579 Melton, M.A.: An analysis of the relation among elements of climate, surface properties and geomorphology, Office of Nav.
580 Res. Dept. Geol. Columbia Univ, NY. Tech. Rep. 11, 1975.

581 Milliken, R.E., Mustard, J.F., Goldsby, D.L.: Viscous flow features on the surface of Mars: observations from high-resolution
582 Mars Orbiter Camera (MOC) images, *J. Geophys. Res.* 108, doi: <https://doi.org/10.1029/2002JE002005>, 2003.

583 Mustard, J.F., Cooper, C.D., Rifkin, M.K.: Evidence for recent climate change on Mars from the identification of youthful
584 near-surface ground ice, *Nature* 412:411–414, doi: <https://doi.org/10.1038/35086515>, 2001.

585 Phillips, J.D., Lutz, J.D.: Profile convexities in bedrock and alluvial streams, *Geomorphology* 102, 554–566, doi:
586 <https://doi.org/10.1016/j.geomorph.2008.05.042>, 2008.

587 Pilorget, C. & Forget: Formation of gullies on mars by debris flows triggered by CO2 sublimation, *Nature Geoscience*, 9, 65–
588 69, doi: <https://doi.org/10.1038/ngeo2619>, 2016.

589 Reiss, D. et al.: Absolute dune ages and implications for the time of formation of gullies in Nirgal Vallis, Mars. *J. Geophys.*
590 *Res.-Planets* 109, doi: <http://dx.doi.org/10.1029/2004JE002251>, 2004.

591 Reiss, D., Hauber, E. et al.: Terrestrial gullies and debris-flow tracks on Svalbard as planetary analogs for Mars, In: Garry,
592 W.B. & Bleacher, J.E. (eds) *Analogues for Planetary Exploration*, *Geol. Soc. Am. Spec. Papers* 483, 165–175, doi:
593 [https://doi.org/10.1130/2011.2483\(11\)](https://doi.org/10.1130/2011.2483(11)), 2011.

594 Rodine, J.D., Johnson, A.M.: The ability of debris, heavily freighted with coarse clastic materials, to flow on gentle slopes,
595 *Sedimentology* 23, 213–234, doi: <https://doi.org/10.1111/j.1365-3091.1976.tb00047.x>, 1976.

596 Ryder, J.: Some aspects of the morphometry of paraglacial alluvial fans in South-central British Columbia, *Canadian Journal*
597 *of Earth Sciences* 8: 1252-1264, doi: <https://doi.org/10.1139/e71-11>, 1971.

598 Schon, S.C., Head, J.W., Fassett, C.I.: Unique chronostratigraphic marker in depositional fan stratigraphy on Mars: Evidence
599 for ca. 1.25 Ma gully activity and surficial meltwater origin, *Geology* 37, 207–210, doi: <http://dx.doi.org/10.1130/g25398a.1>,
600 2009.

601 Siewert, M. B., Krautblatter, M., Christiansen, H. H., & Eckerstorfer, M.: Arctic rockwall retreat rates estimated using
602 laboratory-calibrated ERT measurements of talus cones in Longyeardalen, Svalbard, *Earth Surface Processes and Landforms*,
603 37(14), 1542-1555, doi: <https://doi.org/10.1002/esp.3297>, 2012.

604 Sinha, R. K., Ray, D., De Haas, T., & Conway, S. J.: Global documentation of overlapping lobate deposits in Martian gullies.
605 *Icarus*, 352, 113979, doi: <https://doi.org/10.1016/j.icarus.2020.113979>, 2020.

606 Sinha, R. K., Vijayan, S., Shukla, A. D., Das, P., & Bhattacharya, F.: Gullies and debris-flows in Ladakh Himalaya, India: a
607 potential Martian analogue, *Geol. Soc. Lond. Spec. Publ.* 467, 315-342, doi: <https://doi.org/10.1144/SP46>, 2019.

608 Sinha, R.K., Vijayan, S.: Geomorphic investigation of craters in Alba Mons, Mars: implications for Late Amazonian glacial
609 activity in the region, *Planet. Space Sci.* 144:32–48, doi: <https://doi.org/10.1016/j.pss.2017.05.014>, 2017.

610 Souness, C., & Hubbard, B.: Mid-latitude glaciation on Mars, *Progress in Physical Geography*, 36(2), 238-261, doi:
611 <https://doi.org/10.1177/030913331243>, 2012.

612 Souness, C., Hubbard, B., Milliken, R. E., & Quincey, D.: An inventory and population-scale analysis of martian glacier-like
613 forms, *Icarus*, 217(1), 243-255, doi: <https://doi.org/10.1016/j.icarus.2011.10.020>, 2012.

614 Stock, J.D., Dietrich, W.E.: Erosion of steepland valleys by debris flow, *Geol. Soc. Am. Bull.* 118 (9/10), 1125–1148.
615 doi:10.1130/B25902.1, 2006.

616 Stolle, A., Langer, M., Blöthe, J. H., & Korup, O.: On predicting debris flows in arid mountain belts, *Global and Planetary*
617 *Change*, 126, 1-13, doi: <https://doi.org/10.1016/j.gloplacha.2014.12.005>, 2015.

618 Welsh, A., Davies, T.: Identification of alluvial fans susceptible to debris-flow hazards. *Landslides* 8 (2), 183–194, doi:
619 <https://doi.org/10.1007/s10346-010-0238-4>, 2011.

620 Wilford, D. J., Sakals, M. E., Innes, J. L., Sidle, R. C., & Bergerud, W. A.: Recognition of debris flow, debris flood and flood
621 hazard through watershed morphometrics, *Landslides*, 1(1), 61-66, doi: <https://doi.org/10.1007/s10346-003-0002-0>, 2004.

622 Yue, Z., Hu, W., Liu, B., Liu, Y., Sun, X., Zhao, Q. and Di, K.: Quantitative analysis of the morphology of martian gullies and
623 insights into their formation, *Icarus*, 243, pp.208-221, doi: <https://doi.org/10.1016/j.icarus.2014.08.028>, 2014.

624